

SANDIA REPORT

SAND2012-8539

Unlimited Release

Printed October 2012

Imaging and Quantification of Hydrogen Isotope Trapping

Richard Albert Karnesky, Jr.; Norman C. Bartelt; Derek Huang; Nick Teslich; and Mukul Kumar

Prepared by
Sandia National Laboratories
Albuquerque, New Mexico 87185 and Livermore, California 94550

Sandia National Laboratories is a multi-program laboratory managed and operated by Sandia Corporation, a wholly owned subsidiary of Lockheed Martin Corporation, for the U.S. Department of Energy's National Nuclear Security Administration under contract DE-AC04-94AL85000.

Approved for public release; further dissemination unlimited.



Issued by Sandia National Laboratories, operated for the United States Department of Energy by Sandia Corporation.

NOTICE: This report was prepared as an account of work sponsored by an agency of the United States Government. Neither the United States Government, nor any agency thereof, nor any of their employees, nor any of their contractors, subcontractors, or their employees, make any warranty, express or implied, or assume any legal liability or responsibility for the accuracy, completeness, or usefulness of any information, apparatus, product, or process disclosed, or represent that its use would not infringe privately owned rights. Reference herein to any specific commercial product, process, or service by trade name, trademark, manufacturer, or otherwise, does not necessarily constitute or imply its endorsement, recommendation, or favoring by the United States Government, any agency thereof, or any of their contractors or subcontractors. The views and opinions expressed herein do not necessarily state or reflect those of the United States Government, any agency thereof, or any of their contractors.

Printed in the United States of America. This report has been reproduced directly from the best available copy.

Available to DOE and DOE contractors from

U.S. Department of Energy
Office of Scientific and Technical Information
P.O. Box 62
Oak Ridge, TN 37831

Telephone: (865) 576-8401
Facsimile: (865) 576-5728
E-Mail: reports@adonis.osti.gov
Online ordering: <http://www.osti.gov/bridge>

Available to the public from

U.S. Department of Commerce
National Technical Information Service
5285 Port Royal Rd.
Springfield, VA 22161

Telephone: (800) 553-6847
Facsimile: (703) 605-6900
E-Mail: orders@ntis.fedworld.gov
Online order: <http://www.ntis.gov/help/ordermethods.asp?loc=7-4-0#online>



Imaging and Quantification of Hydrogen Isotope Trapping

Richard Albert Karnesky, Jr.^(a); Norman C. Bartelt^(b)
Derek Huang^(c); Nick E. Teslich, Jr.^(d); and Mukul Kumar^(e)

^(a)Hydrogen and Metallurgical Sciences Department
Sandia National Laboratories
P.O. Box 969
Livermore, California 94550-MS9404

^(b)Materials Physics Department
Sandia National Laboratories
P.O. Box 969
Livermore, California 94550-MS9161

^(c)Materials Science and Engineering Program
Columbia University
500 West 120th Street
New York, New York 10027-MC4701

^(d)Physical & Life Sciences, Chemical Sciences Division
Lawrence Livermore National Laboratory
P.O. Box 808
Livermore, California 94551-L350

^(e)Condensed Matter and Materials Division
Lawrence Livermore National Laboratory
P.O. Box 808
Livermore, California 94551-L370

Abstract

The location of hydrogen isotopes is imaged in austenitic stainless steel and model materials using local-electrode atom-probe (LEAP) tomography and trapping energies are measured by thermal desorption spectroscopy. LEAP tomography has sub-nanometer resolution and excellent compositional sensitivity due to pulse counting techniques. Site-specific sample preparation is possible using focused-ion beam, enabling us to show trapping at low density features, such as

grain boundaries in a model materials (commercially pure nickel and ultra-fine-grain Al-Mg). LEAP tomography is the only known technique to measure trapping to solute atoms (here, nitrogen in 21Cr-6Ni-9Mn austenitic stainless steel), and this report is the first use of the technique to image trapping in austenitic stainless steels. The experimental work is compared with first-principles calculations of the binding energy of hydrogen isotopes to solid solution nitrogen in stainless steels.

ACKNOWLEDGMENTS

It is a pleasure to acknowledge Tom Felter, Dorian Balch, Dean Buchenauer, Michelle Hekmaty, Mark Homer, Doug Medlin, Chris San Marchi, Brian Somerday (SNL) and Dieter Isheim (Northwestern University) for helpful suggestions regarding this work. Sandia National Laboratories is a multi-program laboratory managed and operated by Sandia Corporation, a wholly owned subsidiary of Lockheed Martin Corporation, for the U.S. Department of Energy's National Nuclear Security Administration under contract DE-AC04-94AL85000.

CONTENTS

1. Executive Summary	11
1.1 Project Purpose	11
1.2. Summary of Accomplishments.....	11
1.3. Significance.....	12
2. Introduction.....	13
3. Materials and Methods.....	15
3.1 Materials and Hydrogen Isotope Charging.....	15
3.1.1 21Cr-6Ni-9Mn Stainless Steel.....	15
3.1.2 Grain Boundary Model Materials: Ultra-Fine-Grained Al and Grain-Boundary Engineered, Commercially Pure Ni.....	15
3.1.3 Elevated Temperature, High-Pressure Deuterium Gas Charging	15
3.1.4 Charging During Electropolishing	15
3.1.5 Deuterium Plasma Charging	16
3.2 Thermal Desorption Spectroscopy.....	17
3.3 Local-Electrode Atom-Probe Tomography	18
4. Results and Discussion	23
4.1 Trapping at N in 21-6-9?.....	23
4.1.1 First-Principles Modeling of D-N Binding Energy.....	23
4.1.2 Thermal Desorption Spectroscopy and Trap Energy	23
4.1.3 Local-Electrode Atom-Probe Tomography and Ordering.....	25
4.2 Hydrogen Isotope Trapping at Grain Boundaries of Model Materials	26
5. Summary of Results and Outlook	29
5.1 Conclusions.....	29
5.2 Further Studies	29
6. References.....	31
Distribution	34

FIGURES

Figure 1. A typical thermal desorption spectrum from a sample that has first been charged with gaseous deuterium and then electropolished into a sharpened LEAP needle. Protium from the electropolishing treatment replaces and exceeds deuterium.	16
Figure 2. The Sandia/CA thermal desorption spectrometer.....	17
Figure 3. LEAP tip manufactured by FIB milling.	19
Figure 4. Typical mass/charge spectra from LEAP runs of uncharged (top) and D ₂ charged (bottom) materials. Because of the peak overlap at 2 amu, peak subtraction is used.	20
Figure 5. Typical ramped desorption spectra of 21-6-9 shows trapping due to N and other features.....	24

Figure 6. Summary of the desorption data for 21-6-9 stainless steel with 0.38 wt.% N. Here, we plot the location of a trapping peak at about 0.2 eV, which had steadily increased in height from low-to-high N containing alloys.	24
Figure 7. Experimentally-determined RDF showing a preference for D-N atoms at 0.25nm, which is the distance between neighboring octahedral sites in FCC Fe.	25
Figure 8. Segregation of H (red) and Mg (blue) is observed in LEAP tomography of UFG Al-Mg.	26
Figure 9. Segregation of D (red) and S (black) is observed in LEAP tomography in a commercially pure Ni.	27

NOMENCLATURE

APT	Atom-Probe Tomography
BCC	Body-Centered Cubic
FCC	Face-Centered Cubic
FIB	Focus Ion Beam
GTS	Gas Transfer Systems
LEAP	Local-Electrode Atom Probe
NSC	Nippon Steel Corporation
RDF	Radial Distribution Function
RGA	Residual Gas Analyzer
TDS	Thermal Desorption Spectroscopy

1. EXECUTIVE SUMMARY

1.1 Project Purpose

Hydrogen isotope transport through and embrittlement of pressure vessels ultimately limit component lifetime. Understanding hydrogen interactions with structural materials requires knowing not only equilibrium properties (temperature-dependent lattice solubility, diffusivity, and permeability of hydrogen), but also transient properties. Because it enhances local hydrogen concentration, defect trapping greatly reduces fracture toughness and changes deformation properties. It also makes the apparent diffusivity of hydrogen many orders of magnitude different from the equilibrium lattice diffusivity. However, trapping is typically a weak point in current simulations. Usually, only a single trapping mechanism is assumed at most, while multiple trapping mechanisms operate in real microstructures at temperatures of interest. The experimental characterization of trapping has been limited and has focused on high strength, ferritic steels. Austenitic alloys that are candidate materials and have lower equilibrium permeability values for hydrogen have not been analyzed with the same depth. While the trapping to large features, including grain boundaries and incoherent particles, has been imaged indirectly, smaller features (e.g. precipitates and solute atoms) have not been studied in detail due to fundamental resolution limitations of most analysis techniques.

The location of hydrogen isotopes is imaged in austenitic stainless steel and model materials using local-electrode atom-probe (LEAP) tomography and trapping energies are measured by thermal desorption spectroscopy (TDS). Hydrogen is found to trap to nitrogen solute atoms. LEAP tomography has sub-nanometer resolution and excellent compositional sensitivity due to pulse counting techniques. Site-specific sample preparation is possible using focused-ion beam, enabling us to show trapping at low density features, such as grain boundaries in nickel. These unique capabilities of LEAP tomography make it promising for the study of hydrogen isotopes, but it has not yet been used to image trapping in austenitic stainless steels. The experimental work is compared with first-principles calculations of the binding energy of hydrogen isotopes to solid solution elements in stainless steels and to coherent precipitate/matrix interfaces.

1.2. Summary of Accomplishments

We have imaged directly, for the first time, hydrogen trapping to individual solute atoms. In 21Cr-6Ni-9Mn austenitic stainless steels with varying nitrogen contents, radial distribution functions of our LEAP datasets show short-range ordering of deuterium atoms to nitrogen atoms, with the inter-atomic distance corresponding to the distance between octahedral sites in face-centered-cubic iron. We confirmed the preference of nitrogen and hydrogen isotopes for octahedral sites using first principles calculations. Our thermal desorption spectroscopy measurements have shown that a 0.2 eV/atom deuterium trap has increasing occupancy with increasing nitrogen content. However, this energy is twice the binding energy we calculated for nitrogen and hydrogen using first principles with no magnetic effects considered. With magnetic effects considered, nitrogen seems to repel hydrogen. This suggests the model misses an important contribution, perhaps from vacancies.

Further, we've imaged trapped hydrogen to grain boundaries of both ultra-fine-grained Al-Mg and commercially pure nickel. The amount of solute trapped to the boundaries in nickel seems to depend highly on the nature of the boundary. This may explain the high degree of hydrogen embrittlement observed in as-received nickel that is mitigated by grain boundary engineering.

1.3. Significance

There is no other technique that is currently able to measure hydrogen isotope segregation at length scales below about 100 nm and we have, for the first time, imaged it at sub-nanometer length scales. This new research methodology can be used to understand and model materials intended for hydrogen environments with greater fidelity, with benefits for energy (including both fusion and hydrogen storage, transport, power) and security (e.g. gas transfer systems (GTS)). Further, we have improved the understanding of the specific technical alloys we studied (nitrogen-containing austenitic stainless steel and nickel).

2. INTRODUCTION

In this work, we apply cutting-edge experimental and theoretical techniques to study hydrogen isotope trapping in austenitic stainless steel alloys used in GTS and in model materials in order to advance the technique. Trapping is not characterized well, but greatly impacts the distribution and kinetics of hydrogen isotopes and, ultimately, performance. H is mapped with sub-nanometer resolution in 3-D using LEAP tomography. Complimentary TDS is used to determine trap energies and is compared to first principles models. This allows the measurement of (i) solute-H interactions and of (ii) H behavior and grain and phase boundaries, improving models for H trapping.

H is preferentially trapped at microstructural features in metal [1,2], lowering apparent H diffusivity temporarily (as traps are filled with mobile lattice H), and increasing apparent H solubility. Many two-dimensional techniques have imaged H trapping, including tritium autoradiography, microprinting, and secondary ion mass spectrometry [3]. Each has a resolution limit greater than ca. 100 nm. While they have successfully analyzed trapping to large grain and phase boundaries, they cannot be used to visualize trapping to point defects or nanoscale precipitates. Electron energy-loss spectroscopy (EELS) and energy-filtered transmission electron microscopy (EF TEM) have been used to overcome this spatial resolution [4], but cannot be applied generally and has only been used to visualize ca. 10 nm features. Because LEAP tomography has equal mass sensitivity across the periodic table, has sub-nanometer resolution, and is a 3-D technique, it might be the first methodology to image solute-H interactions. Excellent statistical information from LEAP tomographic analyses may also give more quantitative information on trapping to grain and phase boundaries than conventional techniques (e.g., direct measurement of occupancy).

The Nippon Steel Corporation (NSC) first directly observed H trapping in precipitation-strengthened ferritic steel using LEAP tomography [5,6]. The particular alloy they used is not of direct interest to GTS (due to higher H permeability), but their work was the first proof that LEAP tomography can be used to study hydrogen isotope trapping at the nanometer lengthscale. Sandia's LEAP tomograph has a larger field of view and a pulse repetition rate that is an order of magnitude faster than the instrument at NSC, enabling us to gather larger data sets more quickly. This large amount of data will allow greater statistical certainty for observations of solute-H trapping (the detection efficiency of the LEAP tomograph is only ca. 50%). Novel data analysis techniques, based on nearest-neighbor clustering [7] and radial distribution functions [8] were refined and applied to extract information about solute-H interactions.

3. MATERIALS AND METHODS

3.1 Materials and Hydrogen Isotope Charging

3.1.1 21Cr-6Ni-9Mn Stainless Steel

We have focused our study on 21Cr-6Ni-9Mn (21-6-9), a stable austenitic stainless steel that is alloyed with nitrogen for increased strength. Four heats were used, with 0.24, 0.27, 0.34, and 0.38 wt.% N. An increased N content lowers the stacking fault energy and alloys with greater amounts of N have also had greater amounts of hydrogen embrittlement [9,10]. While nitride precipitates are known to trap H and there is limited evidence that atomic N also acts as a trap [11].

3.1.2 Grain Boundary Model Materials: Ultra-Fine-Grained Al and Grain-Boundary Engineered, Commercially Pure Ni

Hydrogen isotopes are known to trap to grain and phase boundaries in many metals, including FCC Fe [12,13]. However, due to the small analysis volume of LEAP tomography (~100 nm X 100 nm X 500 nm) compared to typical grain sizes (d~1 mm), extracting atom-probe tips containing a boundary can be challenging. To get around this, we have looked at model materials

The grain size of ultra-fine-grained Al-7.5% Mg (UFG Al-Mg, d~200 nm) ensures that analysis volumes of “random” tips will often contain boundaries. The preparation of these materials is documented more completely in Ref. [14]. Focus ion beam milling can create site-specific tips. Due to the high cost of this technique, we focused on grain boundary engineered Ni samples that are of interest to LLNL and SNL and are documented in Ref. [15].

3.1.3 Elevated Temperature, High-Pressure Deuterium Gas Charging

Samples were cleaned using isopropyl alcohol before being inserted into a thick-walled A-286 precipitation-strengthened austenitic stainless steel pressure vessel, located in a furnace. After sealing the pressure vessel, residual gases were removed from the vessel using a sequence of He purging and evacuating. Elevated temperatures enhance diffusion, but also lead to precipitate dissolution or coarsening and other microstructural changes. Charging temperatures of 100 °C and 300 °C were selected to minimize charging times, but still study materials with and without thermally activated microstructure changes. The vessel was backfilled with pure deuterium to 20,000 psi to maximize the amount of deuterium in the specimens.

3.1.4 Charging During Electropolishing

It is common to manufacture atom-probe specimens by electropolishing specimens in perchloric/acetic acid solutions at potentials below 20 V. Due to the high fugacity that arises from the large amount of ionic hydrogen, electrochemical charging is a very common way to charge metal samples at low (ambient) temperatures both more quickly (less than a day instead of weeks or months) and to higher hydrogen content than gas charging. We found here that

protium from electropolishing solutions replaces deuterium introduced by gas charging. Electropolishing in deuterated acids mitigated this replacement and led to increased deuterium in samples. This provides an excellent way to find trap sites, as they become more decorated. However, there is less quantitative certainty in the solubility and trap occupancy measurements, as the exact hydrogen charging conditions during polishing are poorly characterized and non-reproducible, given that the primary goal of polishing is to end in a sharpened metal tip and voltages and charging times are therefore customized on a tip-by-tip basis.

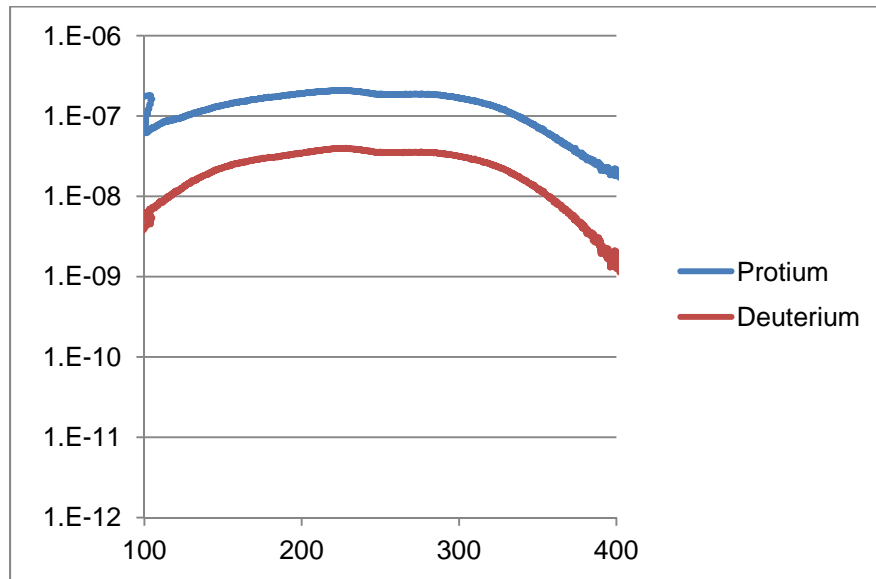


Figure 1. A typical thermal desorption spectrum from a sample that has first been charged with gaseous deuterium and then electropolished into a sharpened LEAP needle. Protium from the electropolishing treatment replaces and exceeds deuterium.

3.1.5 Deuterium Plasma Charging

High-pressure gas charging in accessible lab environments ($\leq 20,000$ psi, ≤ 300 °C) can be time consuming (due to slow equilibrium diffusivity of hydrogen isotopes in steels, large equilibrium solubility values, and trapping). As we demonstrated in our electropolishing work, alternative charging techniques could incorporate larger amounts of hydrogen isotopes in shorter times. Buckley and Birnbaum showed that protium plasmas could be used to charge aluminum samples, achieving atomic concentrations of up to 2880 appm, approximately three times typical levels obtained by electrolytic or chemical charging methods, and without the surface chemistry changes associated with those methods [16]. To test the efficacy of plasma charging, we used a Harrick Plasma Cleaner with an attached Plasmaflo. The Plasmaflo allows for two independent inputs (with independent flow meters) to be flowed into the plasma chamber and also monitors the plasma chamber pressure. For the charging runs, the chamber pressure was kept around 1400-1700 mTorr, with D₂ and Ar inflow pressures of 6 psi each. The plasma cleaner was set to a power of “high”, which nominally corresponds to an RF power of 18 Watts.

Preliminary TDS of plasma charged samples indicates that non-negligible concentrations of hydrogen can be achieved using plasma charging on time scales much shorter than gas charging,

though the concentration of deuterium in the plasma charged samples is lower than those of the gas charged samples.

Charging by plasma preferentially filled higher energy trap sites, namely vacancies. This could be due to inadequate charging conditions: longer charging times may lead to the other trap sites and soluble hydrogen being filled. Or, it could be due to the charging mechanism preferring to create hydrogen isotope-vacancy pairs. Electrochemical and chemical charging are known to create these complexes [17].

Plasma charging seems particularly promising for very small specimens (e.g. atom-probe samples). The hydrogen isotopes used during the treatments and the vacancies are able to redistribute over the smaller cross sections more rapidly, as the diffusion distance scales with the square root of charging time. Because of this, the Sandia LEAP tomograph was fit with a plasma cleaner to allow *in situ* charging. This is a unique and promising capability that will be exploited in the future. In this study, we focus mostly on gas charging, which is still more predictable and quantitative.

3.2 Thermal Desorption Spectroscopy

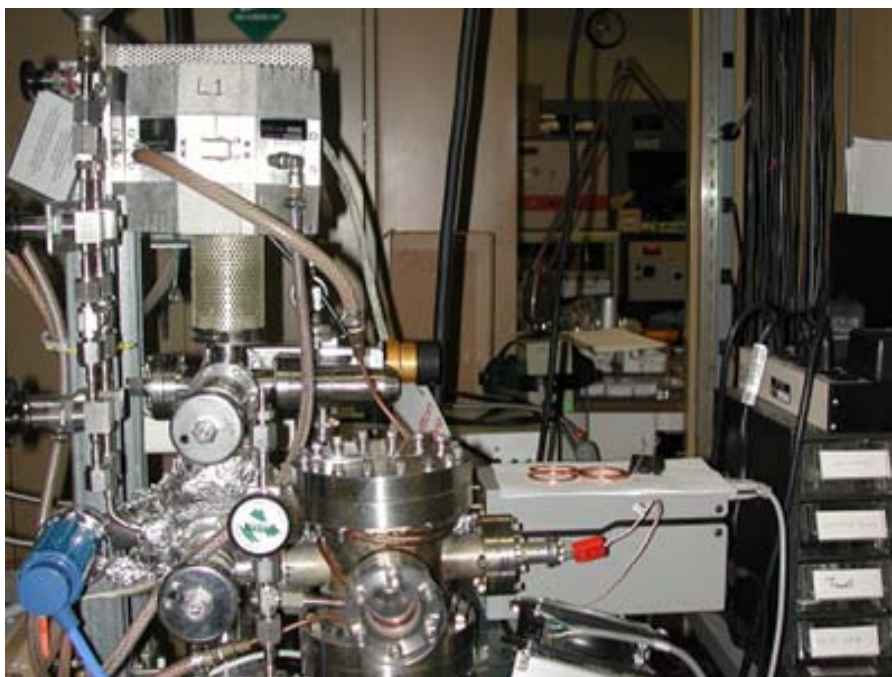


Figure 2. The Sandia/CA thermal desorption spectrometer.

The TDS instrument is an in-house built system that has two segments that can be isolated: a specimen chamber (with a removable quartz thimble, thermocouple, and quartz-lamp furnace), and an analysis chamber (with attached residual gas analyzer (RGA)). The system also employs two vacuum pumps to maintain UHV: a large rotary-vane (RV) backing pump is used to evacuate the specimen chamber without exposing the turbomolecular pump to high gas pressures. Once a sufficiently low background pressure in the specimen chamber is

reached (7-10 mTorr) a gate valve separating the specimen and analysis chambers is opened, allowing the desorbed gas from the sample to be analyzed using the RGA.

Background pressures of 10^{-7} torr were reached before running the analysis. Long pump times may have an effect on the deuterium or hydrogen concentration on the surface (particularly in low-energy trap states) [18], but prolonged pumping of samples does not seem to have a significant effect, as background partial pressures of $<10^{-9}$ torr were maintained throughout pumping and the total amount of desorbed deuterium was measured to be similar during even longer hold times.

The furnace temperature is brought rapidly to 100 °C, and is increased to 1000 °C at a constant ramp rate of between 1 and 10 °C/min.

We employ an Octave [19] script based on a MatLab script by Zhao *et al.* [20] that uses Brownian random search to fit a set of peak parameters to the Polanyi-Wigner equation:

$$r(\Theta) = -\frac{d\Theta}{dt} = \nu\Theta^n \exp\left(-\frac{E_d}{kT}\right),$$

where Θ is the adsorbate fractional coverage, $r(\Theta)$ is the rate of desorption, ν is a frequency factor, n is the order of the desorption process, and E_d is the desorption energy. When multiple peaks convolve and contribute to the total pressure, this expression can be written as:

$$p_{\text{total}}(T) = \frac{KC}{\alpha} \sum_i N_i \nu_i \Theta_i^n \exp\left(-\frac{E_{d,i}}{kT}\right).$$

Note that each peak has an additional factor N (essentially a normalization factor). Also, note that the total pressure equation includes a ramp-rate (α , in units of K/s) dependence.

While this peak fitting method allows for automated fitting of trapping energies using data from a single ramp rate, we also used the fitted peaks in the “heating rate variations” method. The E_d as a function of the peak temperature T_{max} and ramp rate Φ is [18]:

$$\frac{d\ln(\alpha/T_{\text{max}}^2)}{d(1/T_{\text{max}})} = \frac{E_d}{R}.$$

There was good agreement between the two methods of finding desorption energies across different ramp rates and different materials.

3.3 Local-Electrode Atom-Probe Tomography

Most APT tips were prepared by cutting and grinding needles of the aged alloy to square cross sections about 0.3 mm X 0.3 mm. These needles were electropolished in a 10 vol.% perchloric acid in acetic acid solution and then in a solution of 2 vol.% perchloric acid in butoxyethanol. The grain-boundary engineered, commercially pure Ni specimens were manufactured by milling in a dual-beam Focused Ion Beam (FIB)/scanning electron microscope. Grain boundaries were characterized by electron back-scatter diffraction in a scanning electron microscope and

boundaries of different types were marked for analysis. The specimen was stored in liquid nitrogen to minimize deuterium desorption between milling sessions. Platinum was used to attach tips to an array of pre-sharpened tips on a Si wafer and as a protective capping layer in order to prevent Ga ion damage. In order to minimize the chance of deuterium desorption between milling and analysis, we tried a number of different methods (many of which proved unsuccessful. Gold was sputter coated onto the tips, as Au is known to have a very low hydrogen permeation. Unfortunately, this caused electrical arcing on the microtip array, causing damage to all tips on the array. Specimens were stored in a sub-zero freezer, in order to minimize D diffusion. However, this caused condensation when the samples were brought up to ambient temperature outside of vacuum. It was decided to instead run FIB-milled tips within an hour of removing them from the FIB.

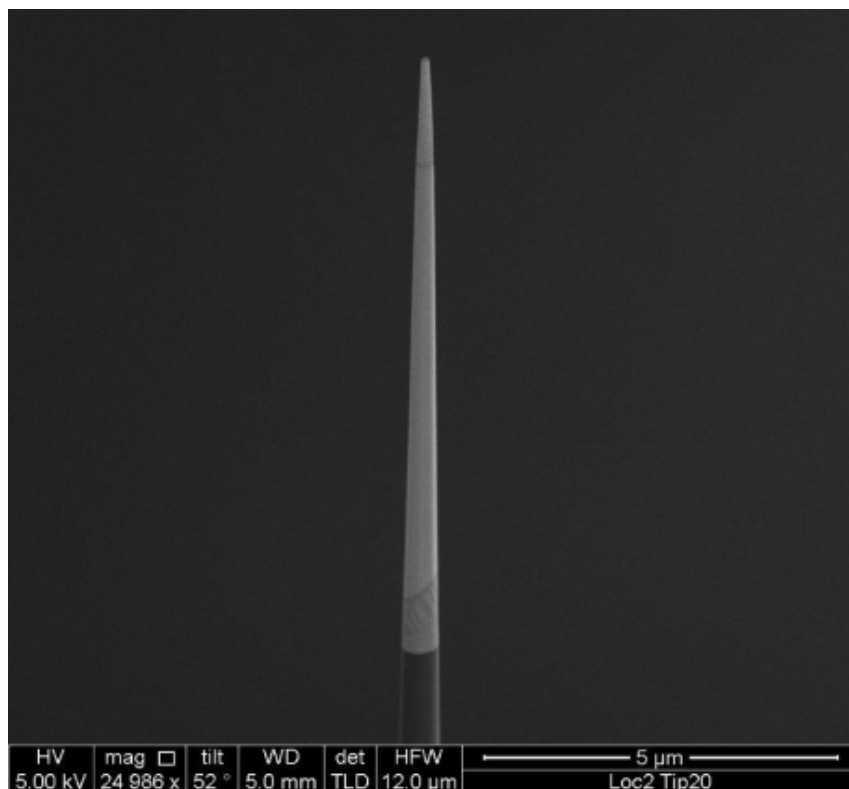


Figure 3. LEAP tip manufactured by FIB milling.

A LEAP 3000 tomograph operating at a specimen temperature of 80 K in the voltage-pulsing mode (20% pulse fraction, as defined by the pulse voltage increment divided by the stationary voltage) was used to collect APT datasets. The LEAP tomograph is modified with two RGAs: one on the specimen buffer chamber, and one in the analysis chamber. These monitored the vacuum system for evidence of outgassing of deuterium from charged specimens. Due to the low vacuum levels, this would be of particular concern in the buffer chamber, as the very thin tips sat at ambient temperature. However, no outgassing was detected. The operating temperature was selected to balance the need to minimize background levels in the mass spectra, but to ensure tip survivability (it is a bit warmer than normal operating conditions, as hydrogen-isotope charged specimens are much more prone to fracture).

The computer program IVAS was used for analysis. Mass ranging of hydrogen isotopes offered some distinct challenges. The most notable of these is that the single D ion peak overlaps with the multi-ion H₂ peak at 2 amu. This was accounted for by assuming a constant H/H₂ ratio is maintained across uncharged and charged materials and subtracting the expected amount of H₂ from the 2 amu peak. This assumption seems reasonable, given that the H/H₂ ratio remains consistent across multiple uncharged specimens when analyzed with the same run conditions.

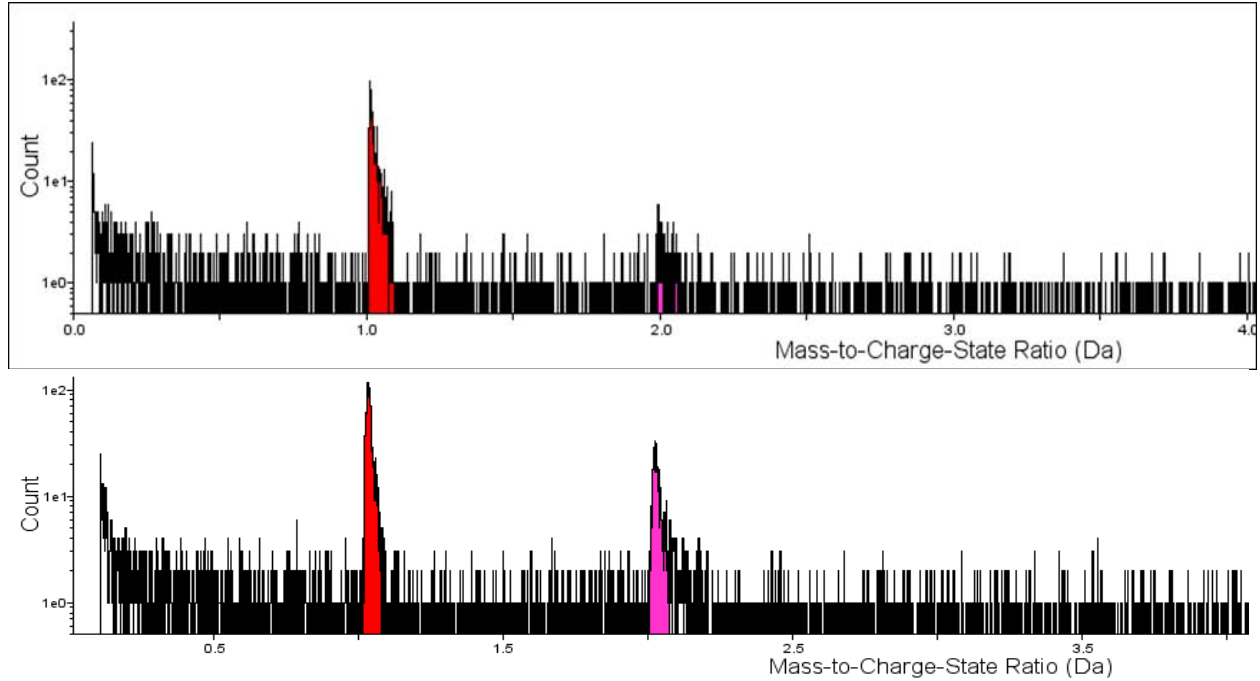


Figure 4. Typical mass/charge spectra from LEAP runs of uncharged (top) and D₂ charged (bottom) materials. Because of the peak overlap at 2 amu, peak subtraction is used.

Because of the low concentration of H or D in the alloy, background subtraction in the m/e spectra is critical to obtain accurate concentrations. Therefore, m/e windows twice as wide as the peak windows were made on either side of a peak (separated from the peak by at least half of the width of each peak's window). Because the total width of background windows is four times the peak width, the background-subtracted concentration is the number of ions in the peak with one fourth of the number of background events subtracted out, divided by the total ranged ions in a spectrum.

A radial distribution function (RDF) provides a concentric concentration profile, centered around a single kind of atom. The RDF at a given radial distance, r , is defined as the average concentration distribution of component i around a given solute species, X , $\langle C_i^X(r) \rangle$, normalized to the total concentration of i atoms, C_i^0 . If the number of i atoms in a shell around the k^{th} X atom is given as $N_i^k(r)$, then:

$$RDF = \frac{\langle C_i^0(r) \rangle}{C_i^0} - 1 = \frac{1}{C_i^0} \sum_{k=1}^{N_x} \frac{N_i^k(r)}{N_{TOT}^k(r)} - 1$$

Typically, the RDF is considered for ≥ 0.2 nm. Below this, there is some contention that possible ion trajectory effects could impact the result. Unity is subtracted to compare the RDF with a random distribution at a value of 0. Positive values indicate a pair preference greater than the overall concentration and negative values indicate a pair repulsion.

4. RESULTS AND DISCUSSION

4.1 Trapping at N in 21-6-9?

N is known to occupy octahedral sites and is a known trap for hydrogen isotopes, which often sit in tetrahedral sites in BCC alloys. In BCC Fe, hydrogen isotopes sit in tetrahedral sites and there is an N-H binding energy of 0.1 eV [21], but there has been no work we're aware of to see if N is a trap in FCC Fe (the structure of austenitic stainless steel). There are some qualitative reasons to believe it would. In FCC Fe, N still occupies octahedral interstitial sites, straining the lattice. Unlike in the BCC structure, H isotopes sit in FCC octahedral sites, and can diffuse through tetrahedral sites [22]. There is a 0.6eV binding energy between H and vacancies in both BCC and FCC Fe [22]

We have measured an increasing D content with increasing N content in the 21-6-9 alloys we have investigated. This can be seen in both an increasing trap occupancy in TDS and a short range ordering between N and D atoms in LEAP tomography. This is supported qualitatively by first principles calculations.

4.1.1 First-Principles Modeling of D-N Binding Energy

Without magnetism, our model obtains a binding energy of 0.104 eV. The 32 Fe-atom unit cell (with a single H and a single N interstitial atoms) is slightly magnetic. With magnetism, the value for the binding energy is weaker: 0.055 eV.

4.1.2 Thermal Desorption Spectroscopy and Trap Energy

Due to multiple possible trapping sites in steel, it can be difficult to fit peaks and assign trapping energies to multiple defects. Multiple peaks are generally not observed, and peaks must be added to the fit in order to fit the overall shape of the desorption spectra. Initial guesses for some peaks can be made based on the locations for peaks expected for vacancies and dislocations. Both of these are generally larger than the desorption energies for peaks that we can possibly attribute to trapping at solutes of different kinds. Because we have material which is nominally quite similar, with a single varying quantity (nitrogen content), we look for peaks that vary systematically across all four specimens, based on the amount of N.

There is a low energy peak, at 0.2 eV, that increases monotonically with increasing N content. This value is 2-4 times that predicted by the model. The reason for this discrepancy is not clear. We could be mis-attributing the peak in the experimental data. Several other solute atoms are predicted to have binding energies of about 0.2 eV in Fe. This would require the monotonic increase in the peak height with increasing N content that we observed be fortuitous, though. Our ability to discern lower energy peaks is limited, due to the relatively large H-Fe interstitial binding energy, the difficulty of starting thermal ramps below 100 C, and the dominance of higher energy peaks in the data. The model could also be improved. We could look at larger unit cells or we could consider the effects of vacancies and other solute atoms. In particular, the literature predicts short range ordering of N with some substitutional species (particularly Cr). We did not attempt to model binding between Cr-N, Cr-H, or Cr-H-N yet.

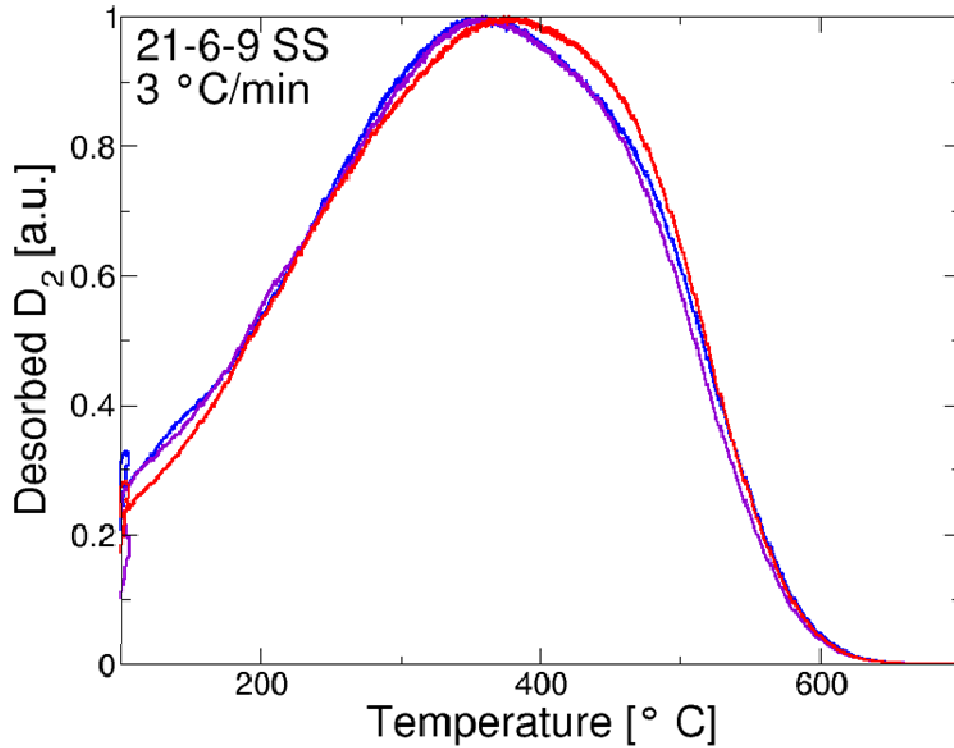


Figure 5. Typical ramped desorption spectra of 21-6-9 shows trapping due to N and other features.

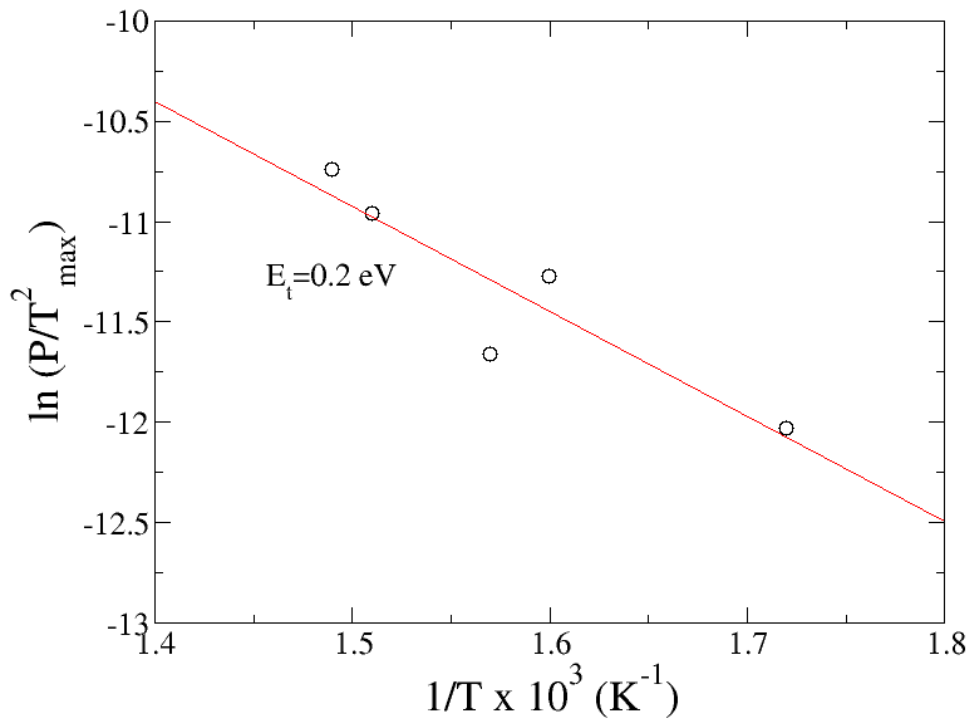


Figure 6. Summary of the desorption data for 21-6-9 stainless steel with 0.38 wt.% N. Here, we plot the location of a trapping peak at about 0.2 eV, which had steadily increased in height from low-to-high N containing alloys.

4.1.3 Local-Electrode Atom-Probe Tomography and Ordering

There is no D segregation that is visually obvious in LEAP tomographic datasets of these materials. Macro-segregation is small enough that the total deuterium content measured by LEAP tomography is within the experimental uncertainty of the deuterium measured by thermal desorption. There is ordering observed between D and N using the RDF, though. The peak observed in the RDF is at 0.25 nm is the distance between two octahedral sites in the FCC Fe lattice. Further from this peak, there seems to be less D near N than would be predicted in a random solution until about 2 nm, where there seems to be no ordering at longer ranges.

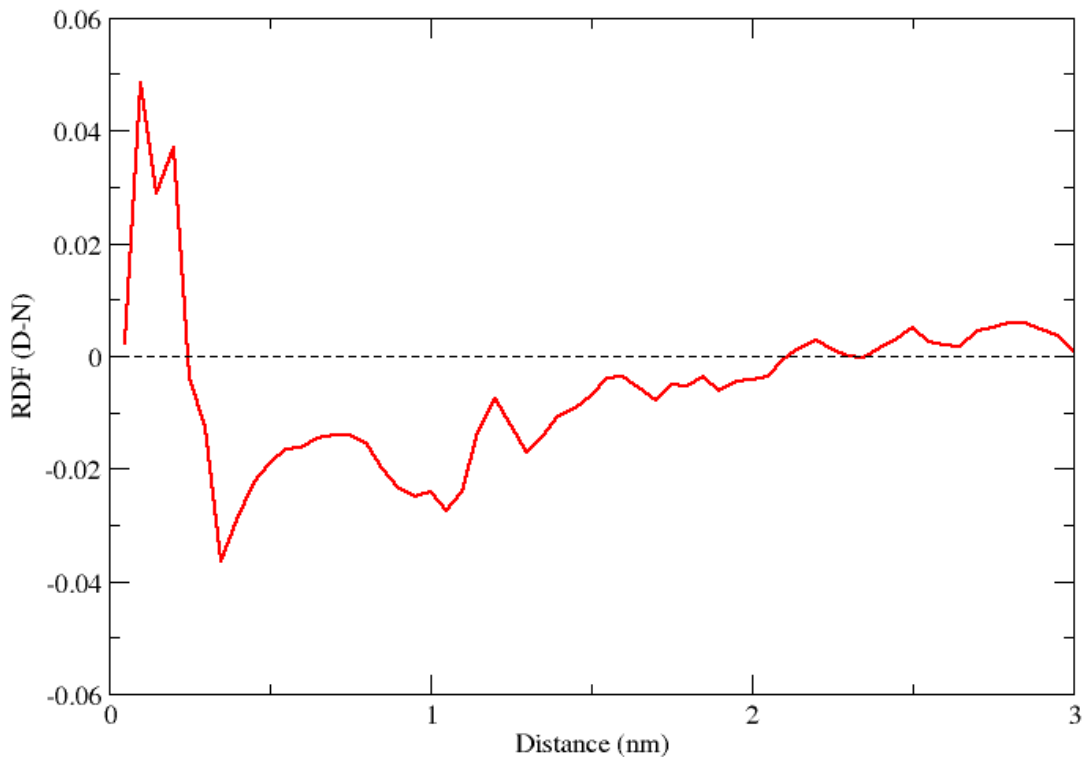


Figure 7. Experimentally-determined RDF showing a preference for D-N atoms at 0.25nm, which is the distance between neighboring octahedral sites in FCC Fe.

Using this RDF methodology, we will be able to measure possible short range ordering of N to, e.g. Cr. This has not yet been completed due to computational time and the larger concentration of Cr atoms to poll.

4.2 Hydrogen Isotope Trapping at Grain Boundaries of Model Materials

We measure both Mg and H (protium) segregation to grain boundaries in UFG Al-Mg. It remains to be seen whether this segregation is due to trapping by the boundaries, by (most likely atomic) Mg, or some combination of the two. In order to test this further, we would need to look at alloys with varying amounts of Mg segregation to the boundaries (most likely by looking at different overall compositions, but we can also change segregation and grain size through thermally aging the samples).

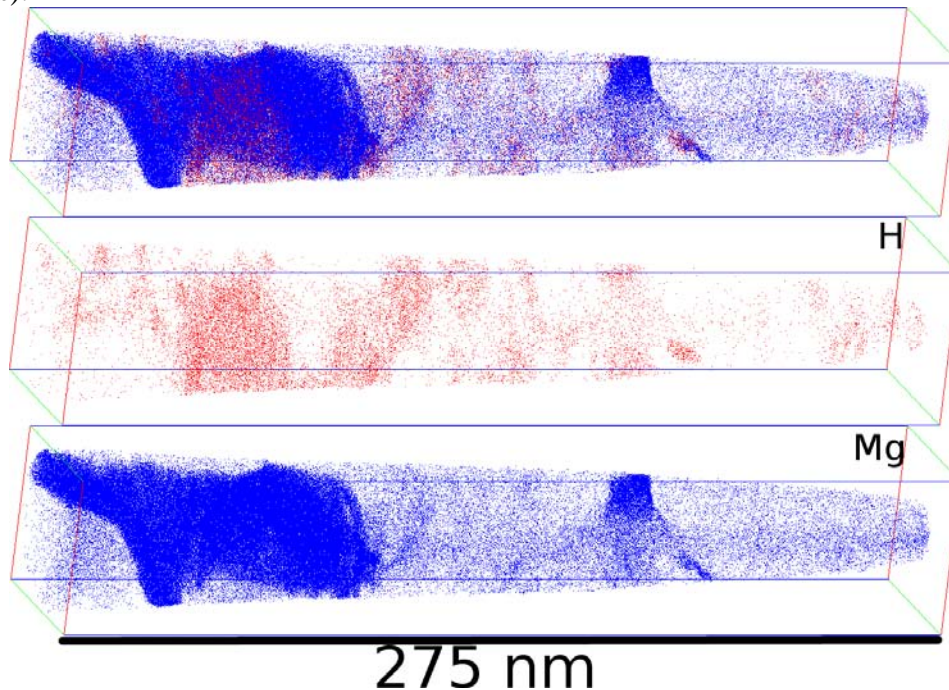


Figure 8. Segregation of H (red) and Mg (blue) is observed in LEAP tomography of UFG Al-Mg.

Two types of Ni grain boundaries were analyzed. A twin boundary did not have any measurable D. A boundary of random orientation showed both S and D segregation. Because segregation can vary widely with the five degrees-of-freedom in grain boundaries [23], further analysis would be needed to gain a statistically significant amount of information from a variety of grain boundaries in Ni. Similarly to the case of UFG Al-Mg, it remains to be seen if hydrogen isotopes trap at boundaries, at impurity atoms that also segregate to the boundaries, or both.

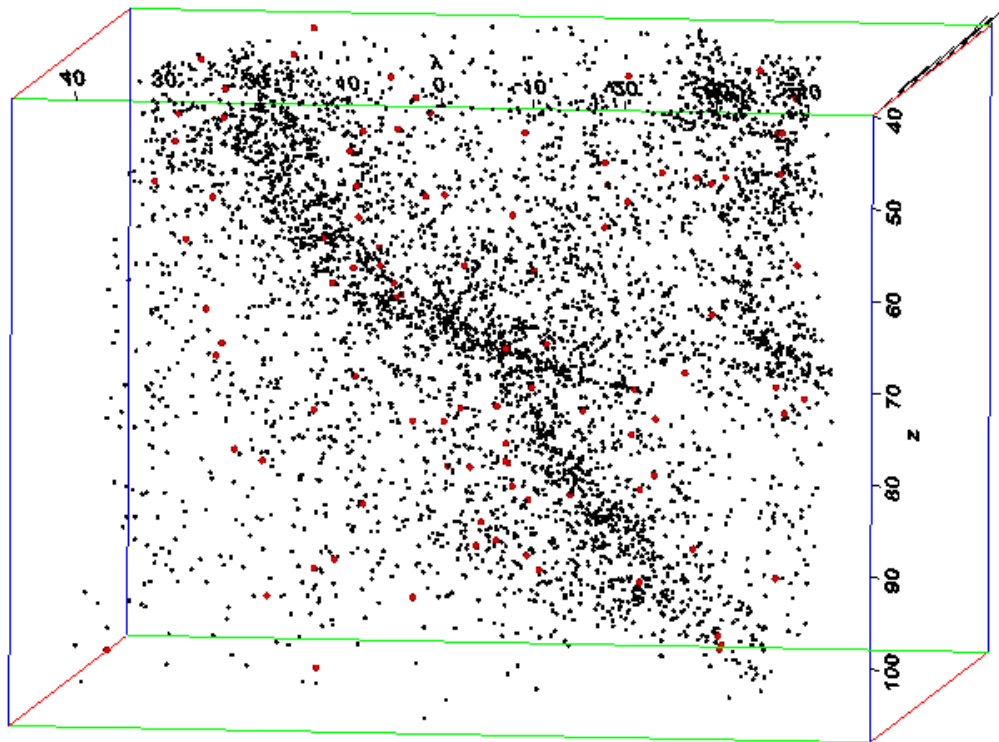


Figure 9. Segregation of D (red) and S (black) is observed in LEAP tomography in a commercially pure Ni.

5. SUMMARY OF RESULTS AND OUTLOOK

5.1 Conclusions

We have demonstrated that LEAP tomography is effective at analyzing the distribution of deuterium when present at parts-per-million or greater levels, as is typical for many charged specimens. We have observed:

- Short-range ordering of deuterium to nitrogen, sitting in adjacent octahedral interstitial sites in 21-6-9 stainless steel, in agreement with first principles modeling
- Segregation of deuterium and sulfur to “non-special” grain boundaries in grain-boundary engineered, commercially-pure Ni
- Grain boundary segregation of Mg and H in UFG Al-7.5% Mg.

We have also come to the following conclusions from TDS data:

- Protium can replace deuterium introduced during gas charging when LEAP tomograph specimens are electropolished
- The magnitude of a 0.2 eV/atom trap increases with increasing N content. This is twice the energy calculated from first principles with no magnetic effects.

5.2 Further Studies

This early career LDRD demonstrates that TDS and LEAP tomography are powerful complimentary techniques to study hydrogen isotope trapping in metals. We are currently trying to answer the following questions:

- Is there short range ordering of N to elements within the steels (e.g. Cr)?
- What is the origin of other trapping energies we measured by TDS?
- What might explain the differences of binding energies measured in TDS and calculated by first principles?
- In the model materials used to study grain boundaries, is there hydrogen isotope segregation to the boundary itself, the other elements (e.g. S, Mg) that decorate the some boundaries, or some combination of the two?

These techniques also hold promise to look at trapping in other alloys of interest to GTS. In particular, we intend to study the precipitation-strengthened Al-Cu system. This provides the basis for the 2000-series candidate alloys. Reports on trapping in these systems have been inconsistent. The hydrogen isotope content in binary Al-4 wt.% Cu was several times higher than that of pure Al, although binary Al-Cu alloys generally have low hydrogen contents compared to those with elements that are known to trap more effectively (e.g. Mg and Li) [24]. The binding energy of H to Cu in solution has previously been bounded as ≤ 0.05 eV [25]. Al-Cu GP-zones and precipitates have been observed by tritium autoradiography to trap hydrogen isotopes [26], but there have not been significant trap energies measured in Al-Cu binaries by TDS [24].

6. REFERENCES

1. C. San Marchi, B. P. Somerday, and S. L. Robinson, Permeability, Solubility and Diffusivity of Hydrogen Isotopes in Stainless Steels at High Gas Pressures, in *International Journal of Hydrogen Energy*, Vol. 32, No. 1, pp. 100–16, 2007.
2. R. A. Oriani, The Physical and Metallurgical Aspects of Hydrogen in Metals, in *Fusion Technology*, Vol. 26, No. 4, pp. 235–66, 1994.
3. K. Kawamoto, Y. Oda, H. Noguchi, H. Fujii, T. Izumi, and G. Itoh, Investigation of Local Hydrogen Distribution Around Fatigue Crack Tip of a Type 304 Stainless Steel with Secondary Ion Mass Spectrometry and Hydrogen Micro-print Technique, in *Journal of Solid Mechanics and Materials Engineering*, Vol. 3, No. 6, pp. 898–909, 2009.
4. K. Tatsumi, S. Muto, and T. Yoshida, Detection of Hydrogen at Localized Regions by Unoccupied Electronic States in Iron Carbides: Towards High Spatial Resolution Mapping of Hydrogen Distributions, in *Journal of Applied Physics*, Vol. 101, No. 2, p. 023523, 2007.
5. J. Takahashi, K. Kawakami, Y. Kobayashi, and T. Tarui, The First Direct Observation of Hydrogen Trapping Sites in TiC Precipitation-hardening Steel Through Atom Probe Tomography, in *Scripta Materialia*, Vol. 63, No. 3, pp. 261–4, 2010.
6. J. Takahashi, K. Kawakami, and T. Tarui, Direct Observation of Hydrogen-trapping Sites in Vanadium Carbide Precipitation Steel by Atom Probe Tomography, in *Scripta Materialia*, Vol. 67, No. 2, pp. 213–6, 2012.
7. T. Philippe, F. De Geuser, S. Duguay, W. Lefebvre, O. Cojocar-Mirédin, G. Da Costa, and D. Blavette, Clustering and Nearest Neighbour Distances in Atom-probe Tomography, in *Ultramicroscopy*, Vol. 109, No. 10, pp. 1304–9, 2009.
8. D. Haley, T. Petersen, G. Barton, and S. P. Ringer, Influence of Field Evaporation on Radial Distribution Functions in Atom Probe Tomography, in *Philosophical Magazine*, Vol. 89, No. 11, p. 925, 2009.
9. A. W. Thompson, J. A. Brooks, and A. J. West, The Effect of Hydrogen on Mechanical Behavior of Nitrogen-strengthened Stainless Steel, in *Proceedings of an International Conference on Effect of Hydrogen on Behavior of Materials*, pp. 116–25, 1976.
10. R. E. Stoltz and J. B. Sande, The Effect of Nitrogen on Stacking Fault Energy of Fe-Ni-Cr-Mn Steels, in *Metallurgical Transactions A*, Vol. 11, No. 6, pp. 1033–7, 1980.
11. S. Ningshen, M. Uhlemann, F. Schneider, and H. S. Khatak, Diffusion Behaviour of Hydrogen in Nitrogen Containing Austenitic Alloys, in *Corrosion Science*, Vol. 43, No. 12, pp. 2255–64, 2001.
12. P. M. Abraham, T. S. Elleman, and K. Verghese, Diffusion and Trapping of Tritium in Grainboundaries of 304L Stainless Steel, in *Journal of Nuclear Materials*, Vol. 73, No. 1, pp. 77–88, 1978.

13. R. D. Calder, T. S. Elleman, and K. Verghese, Grain Boundary Diffusion of Tritium in 304-and 316-stainless Steels, in *Journal of Nuclear Materials*, Vol. 46, No. 1, pp. 46–52, 1973.
14. C. San Marchi, A. Brown, G. Lucadamo, R. Karnesky, and N. Y. C. Yang, *Physical and Mechanical Metallurgy of Nanostructured Aluminum Alloys*, Sandia National Laboratories, Livermore, CA, 2008.
15. S. Bechtle, M. Kumar, B. P. Somerday, M. E. Launey, and R. O. Ritchie, Grain-boundary Engineering Markedly Reduces Susceptibility to Intergranular Hydrogen Embrittlement in Metallic Materials, in *Acta Materialia*, Vol. 57, No. 14, pp. 4148–57, 2009.
16. C. E. Buckley, H. K. Birnbaum, J. S. Lin, S. Spooner, D. Bellmann, P. Staron, T. J. Udovic, and E. Hollar, Characterization of H Defects in the Aluminium–Hydrogen System Using Small-Angle Scattering Techniques, in *Journal of Applied Crystallography*, Vol. 34, No. 2, pp. 119–29, 2001.
17. H. K. Birnbaum, C. Buckley, F. Zeides, E. Sirois, P. Rozenak, S. Spooner, and J. S. Lin, Hydrogen in Aluminum, in *Journal of Alloys and Compounds*, Vol. 253-254, pp. 260–4, 1997.
18. G. A. Young and J. R. Scully, The Diffusion and Trapping of Hydrogen in High Purity Aluminum, in *Acta Materialia*, Vol. 46, No. 18, pp. 6337–49, 1998.
19. J. W. Eaton, D. Bateman, and S. Hauberg, *GNU Octave Manual Version 3*, Network Theory Ltd., 2008.
20. X. Zhao, R. A. Outlaw, J. J. Wang, M. Y. Zhu, G. D. Smith, and B. C. Holloway, Thermal Desorption of Hydrogen from Carbon Nanosheets, in *The Journal of Chemical Physics*, Vol. 124, No. 19, p. 194704, 2006.
21. A. I. Shirley and C. K. Hall, Trapping of Hydrogen by Substitutional and Interstitial Impurities in α -Iron, in *Scripta Metallurgica*, Vol. 17, No. 8, pp. 1003–8, 1983.
22. B.-J. Lee and J.-W. Jang, A Modified Embedded-atom Method Interatomic Potential for the Fe–H System, in *Acta Materialia*, Vol. 55, No. 20, pp. 6779–88, 2007.
23. D. W. Krakauer and D. N. Seidman, Subnanometer Scale Study of Segregation at Grain Boundaries in an Fe(Si) Alloy, in *Acta Materialia*, Vol. 46, No. 17, pp. 6145–61, 1998.
24. S. Smith and J. Scully, The Identification of Hydrogen Trapping States in an Al-Li-Cu-Zr Alloy Using Thermal Desorption Spectroscopy, in *Metallurgical and Materials Transactions A*, Vol. 31, No. 1, pp. 179–93, 2000.
25. Y. Iijima, S.-I. Yoshida, H. Saitoh, H. Tanaka, and K.-I. Hirano, Hydrogen Trapping and Repelling in an Al-6 Wt % Zn-2 Wt % Mg Alloy, in *Journal of Materials Science*, Vol. 27, No. 21, pp. 5735–8, 1992.

26. H. Saitoh, Y. Iijima, and K. Hirano, Behaviour of Hydrogen in Pure Aluminium, Al-4 Mass% Cu and Al-1 Mass% Mg₂Si Alloys Studied by Tritium Electron Microautoradiography, in *Journal of Materials Science*, Vol. 29, No. 21, pp. 5739–44, 1994.

DISTRIBUTION

1	M0931	W. Ballard	08200
1	MS0899	Technical Library	9536 (electronic copy)
1	MS0359	D. Chavez, LDRD Office	1911



Sandia National Laboratories